

# Optimized apertureless optical near-field probes with 15 nm optical resolution

H G Frey<sup>1</sup>, C Bolwien<sup>2</sup>, A Brandenburg<sup>2</sup>, R Ros<sup>1</sup> and D Anselmetti<sup>1,3</sup>

<sup>1</sup> Bielefeld University, Experimental Biophysics and Applied Nanoscience, Universitätsstraße 25, 33615 Bielefeld, Germany

<sup>2</sup> Fraunhofer Institute for Physical Measurement Techniques IPM, Heidenhofstraße 8, 79110 Freiburg, Germany

E-mail: [dario.anselmetti@physik.uni-bielefeld.de](mailto:dario.anselmetti@physik.uni-bielefeld.de)

Received 13 December 2005

Published 5 June 2006

Online at [stacks.iop.org/Nano/17/3105](http://stacks.iop.org/Nano/17/3105)

## Abstract

Back-illuminated full body glass tips coated with a thin metal layer can be used as local probes for apertureless scanning near-field optical microscopy (SNOM). In order to achieve high spatial resolution, high electric field intensities and low background illumination, the thickness of the metal coating, angular illumination direction, and polarization have to be optimized. Optimal conditions have been calculated and experimentally verified for 10–15 nm thick aluminium and 15–25 nm thick silver layers. Upon imaging single dye molecules, characteristic single and double-peak patterns with peak widths down to 15 nm could be measured, exhibiting an optical resolution which exceeds the classical diffraction limit of Abbé significantly.

(Some figures in this article are in colour only in the electronic version)

## 1. Introduction

Scanning near-field optical microscopy [1, 2] (SNOM) strives for the highest optical resolution, i.e. significantly beyond the classical diffraction limit of Abbé, and simultaneously provides optical and topographical information. In fluorescence SNOM, the sample is locally illuminated by the strongly confined near-field of an optical probe, which is brought in close proximity to the sample. The fluorescence is detected in the optical far field.

Efficient and successful single molecule fluorescence imaging combines high optical intensities, high signal-to-noise ratio and high spatial resolution. In conventional fibre-optic SNOM, where light confinement is realized with a nanometre-sized aperture in a metal coated fibre tip, these issues are very difficult to combine, since a small aperture (<50 nm) is normally characterized by an extremely low light throughput. Recently, interesting concepts for high resolution fluorescence imaging have been published with new kinds of probes, such as the tip-on-aperture (TOA) probe [3] or apertureless probes with external illumination [4, 5]. However, both techniques suffer from fundamental drawbacks since the

TOA probe is difficult to prepare, and the apertureless probe with external illumination suffers from an intense background illumination, quickly bleaching dye molecules and giving rise to a large background signal. In this paper, we investigate optical cantilever probes with an integrated and completely metal coated full body glass tip, which are illuminated from the back side. It has already been shown that such probes can be used for fluorescence near-field imaging [6–8], and interesting concepts for local field enhancements due to tapered plasmonic waveguides have recently been proposed [9–14]. In the experimental studies, rather thick (60 nm) aluminium or iridium layers have been applied limiting the achievable optical and topographical resolution and light throughput. The goal of this paper is to achieve higher spatial resolution by optimizing illumination conditions and metal layer thicknesses.

## 2. Materials and methods

In our SNOM experiment, we investigated Si<sub>3</sub>N<sub>4</sub> contact mode cantilevers (stress-free Si<sub>3</sub>N<sub>4</sub> deposited by plasma enhanced chemical vapour deposition (PECVD), length 350 μm, spring constant 50 mN m<sup>-1</sup>) with an integrated full body glass tip (doped SiO<sub>2</sub> deposited by PECVD, length of the tip: 7 μm),

<sup>3</sup> Author to whom any correspondence should be addressed.

which have been coated using standard thermal evaporation. When metal coated, the  $\text{Si}_3\text{N}_4$  cantilever becomes a nearly opaque screen protecting the sample from direct illumination.

Our theoretical simulations were performed with a multiple multipole simulation program (MMP) [15] in Matlab 6.0 (MathWorks). To reduce complexity, a total tip height of about  $2\ \mu\text{m}$  and an infinite screen of an ideal metal for simulating the metal coated cantilever are assumed. The calculations were done assuming rotational symmetry of probe and fields and in the absence of the normally present glass surface.

Although the chosen boundary conditions for simulation are a simplistic model compared with a real tip geometry, it might serve as a reasonable model in order to qualitatively and semiquantitatively characterize its optical properties. The overall curvature of the model tip (figure 1(a)) with a typical tip radius of 10 nm was fitted to the measured front part of the tips which has been determined by electron microscopy (figure 1(b)). A total opening angle of  $40^\circ$  has been assumed, however, this angle sometimes varies between  $35^\circ$  and  $70^\circ$  for real probes. A superposition of incoming plane waves of equal amplitudes from all horizontal directions under the inclination angle  $\vartheta$  was considered as the illumination source. A radially polarized illumination [13] was assumed in order to achieve high field concentration at the tip apex (figure 1(c)). In this case, all horizontal electric field components vanish at any point of the  $z$ -axis. Although our experimental illumination is approximately given by a single plane wave, the chosen model can account for it. This has been verified by additional simulations for simpler tip geometries showing that the near-field along the  $z$ -axis of a metal tip is dominated by the  $z$ -component of the electric field (data not shown). Due to the rotational symmetry, the  $z$ -component of the electric field yields the same dependence on the inclination angle and on the metal layer thickness.

All of the calculations are based on a laser wavelength of  $\lambda = 532\ \text{nm}$ , corresponding to the diode pumped solid-state laser module used in our experiment (CrystaLaser GCL-025-L). For coating materials, aluminium (Al) and silver (Ag) with their tabulated dielectric constants  $\epsilon_{\text{Al}} = -40.1 + 12.4\ i$  and  $\epsilon_{\text{Ag}} = -12.14 + 1.73\ i$  [16] have been chosen because of their small penetration depths and long surface plasmon decay lengths.

### 3. Simulation results

In figure 2, the calculated electric field intensity distribution ( $|E|^2$ ) is exemplarily shown for a 10 nm Al coated glass tip under an illumination angle of  $\vartheta = 12^\circ$ . The spatial distribution of  $|E|^2$  is given in a logarithmic grey scale representation (figure 2(a)) and the electrical field vectors at the tip end are indicated by the length and orientation of the lines (figure 2(b)). It is noteworthy that the electric field distribution resembles that of an externally illuminated apertureless probe [5], demonstrating the expected electric field confinement at the tip apex. When imaging single fluorescent molecules, the excitation of the molecules is proportional to the square of the electrical field component parallel to their transition dipole moments. For this reason, the calculated field distribution (figure 2(b)) below the tip leads to

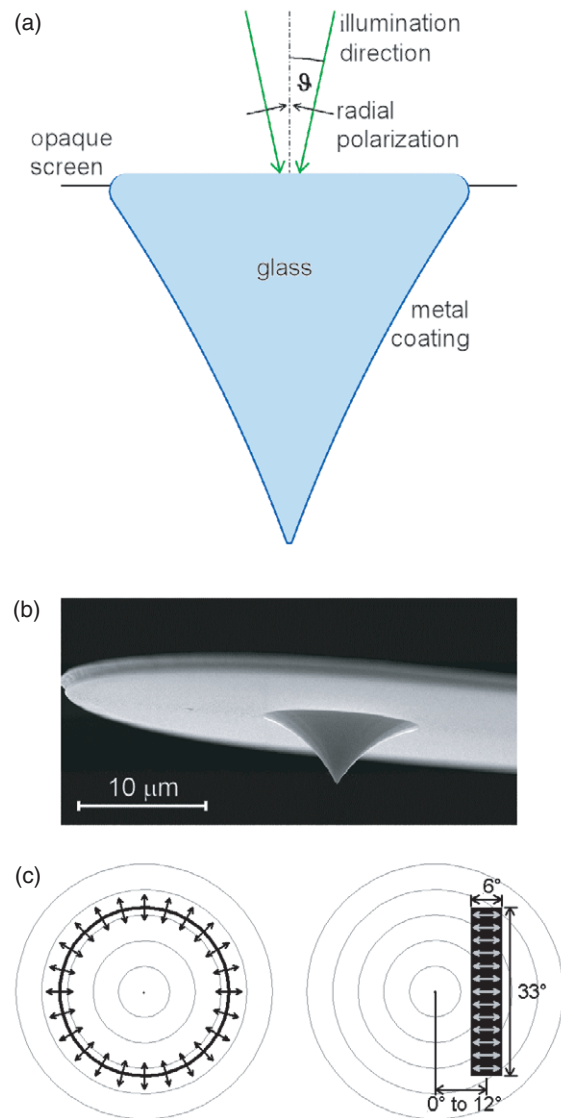


**Figure 1.** (a) Apertureless full body glass tip with 10 nm metal coating thickness used for model calculations. The length of the glass tip is 2035 nm. The tip is illuminated by the superposition of incoming plane waves from all horizontal directions under the inclination angle  $\vartheta$  with radial polarization. (b) SEM image of a metal coated SNOM probe showing the end of the  $\text{Si}_3\text{N}_4$  lever and the glass tip. (c) Comparison of the illumination conditions in theory (left) and experiment (right) shown as windows (black) in the numerical aperture plot. The arrows indicate the polarization direction.

a double peaked fluorescence pattern for dye molecules with horizontal transition dipole moments [3].

In order to investigate the dependence of the electric field intensity concentration ( $|E|^2$ ) at the tip apex on metal layer thickness and illumination angle, many MMP simulations were done and the results are plotted in figure 3. In figure 3(a), a set of exemplified curves for Al coated tips is shown where the illumination angle has been varied from  $\vartheta = 0^\circ$  to  $90^\circ$ . The angles which correspond to the maximum of the individual curves have been determined and plotted, together with their relative intensities, against the metal coating thickness (figures 3(b) and (c)). For an Al coated tip, a

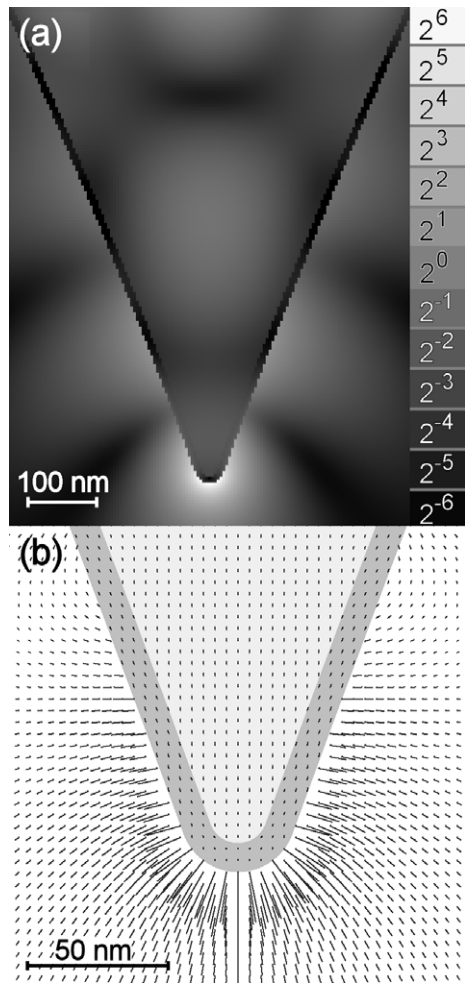


**Figure 2.** Calculated electric field distribution according to MMP theory (parameters: 10 nm Al,  $\vartheta = 12^\circ$ ). (a) The distribution of  $|E|^2$  in logarithmic scale (a.u.) and (b) directions of the electrical field at the tip apex (snapshot at the moment of strongest tip fields). Length and direction of the electric field vectors is indicated by the length and orientation of the short lines.

steep and short-range increase in electric field intensity with a maximum around 5 nm coating thickness and an immediate intensity decrease for larger values is observed (figure 3(b)). In contrast to this finding, a Ag coated tip yields a maximum intensity of the electric field at 25 nm coating thickness (figure 3(c)).

As can be seen from figure 3(a), the angular distribution of the relative intensity is rather broad (up to  $36^\circ$  at 10 nm aluminium). It is noteworthy that focusing a broad angular light cone unfortunately does not necessarily lead to a substantial positive effect unless the phase shift between the individual angular contributions (figure 3(d)) is compensated.

Aside from the absolute value of the electrical field intensity, its decay with lateral displacement is also essential for characterizing properties such as optical resolution and signal-to-background ratio. We have calculated the lateral decay of the electric field intensity ( $|E|^2$ ) from the tip centre for the optimized angles of illumination as determined in figure 3(b) for glass tips coated with 0, 10 and 40 nm of Al which are plotted on a logarithmic scale in figure 3(e). The

corresponding full widths at half maxima (FWHM) can be used as an estimate of the theoretical lateral resolution and are plotted accordingly in figure 3(f). These FWHM values exhibit a linear dependence on the metal layer thickness and compare very well with the anticipated tip radius model where the effective radius is composed of a glass tip radius (10 nm) and coating thickness. It can be inferred from this scheme, that upon using Al coated glass tips, an optical resolution below 20 nm can theoretically be achieved with metal coating thicknesses below 10 nm.

The observed phenomena can be explained in the framework of surface plasmon polaritons, where light can couple through the thin metal coating to surface plasmons on its outer surface. These plasmons propagate along the probe towards the tip, where they are reflected and give rise to standing waves (figure 2). For thin metal layers, the propagation wavevector (real and imaginary part) of surface plasmons strongly depends on the layer thickness [17]. Therefore, the illumination angle which ensures optimal k-matching and hence optimal coupling to surface plasmons depends on the layer thickness. For very thin metal layers, the damping of the surface plasmons and also the leakage of light are strong, yielding only weak confinement of the optical fields at the tip apex. On the other hand, for rather thick metal layers the coupling of light to surface plasmons is weak, indicating optimal conditions at intermediate metal layer thicknesses.

#### 4. Experimental results

The theoretical concept has been tested in SNOM experiments on single dye molecules with a dedicated setup which has recently been published [18], and which was modified by introducing a new SNOM head capable of using cantilever based optical probes. In contrast to the simulations, the experimental setup is restricted to an asymmetric and unidirectional illumination. For this case of asymmetric illumination, we also expect the near-field electric field intensity distribution at the tip apex to be of asymmetric form. The range of the experimentally accessible inclination angles is  $0^\circ$ – $12^\circ$ .

In order to statistically evaluate the importance of the metal layer, the same tip has been coated successively with a set of different layers: 14 nm Al, 27 nm Al, 41 nm Al, 22 nm Ag and 55 nm Ag. Prior to every probe preparation, the Al layers were always removed by (diluted) KOH etching. All of these tips were investigated in SNOM experiments where dye molecules (Alexa 532, Molecular Probes) were immobilized on a glass surface at the highest dilution. In figures 4(a)–(c), fluorescence SNOM patterns of single dye molecules are shown. Each image corresponds to an area of  $1.25 \mu\text{m} \times 2 \mu\text{m}$  and was taken with the identical glass core tip coated with different metal layers: (a) 14 nm Al, (b) 27 nm Al, and (c) 22 nm Ag. In all three SNOM images, individual Alexa 532 dye molecules can be detected by the known characteristic double-peak fluorescence pattern of single molecules, often exhibiting an asymmetric shape clearly proving the single molecule imaging capabilities of our optical probes. From these fluorescence patterns, the orientation of the transmission dipole moments can be recalculated [3], taking quenching [15] and antenna effects induced by the tip into

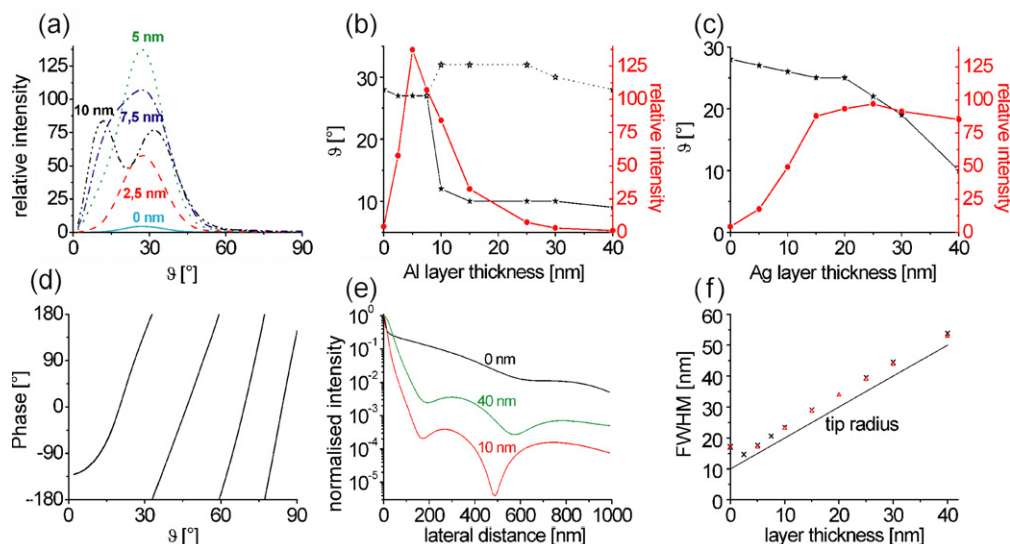


**Figure 3.** (a) Dependence of the electrical field intensity ( $|E|^2$ ) at the tip apex on the inclination angle  $\vartheta$  of the illumination. Exemplarily, the curves for 0, 2.5, 5, 7.5 and 10 nm thick Al coated probes are shown. For Al layers thicker than 7.5 nm a bifurcation into two peaks is apparent. (The normalization of the intensity is chosen in a way that the numbers approximately correspond to the intensity enhancement, when the probe is illuminated with a single plane wave.) (b) Al coated glass tip: optimized illumination angle (star) and the corresponding intensity (circle) are given with respect of the Al layer thickness. The dotted line indicates the angle of the second smaller local maximum. (c) The same as (b) but for Ag coated glass tips. (d) The phase of the electrical field at the tip apex as function of the inclination angle  $\vartheta$  (for 10 nm Al coating). (e) Lateral decay of the electrical field intensity ( $|E|^2$ ) (normalized to 1 at the tip apex) as a function of the lateral distance from the tip apex. The three curves are calculated for 0, 10 and 40 nm Al coating. (f) FWHM of the lateral decay of the normalized electrical field intensity as a function of the metal layer thickness. Ag (triangles) and Al ( $\times$ ) coatings for the same tip radius give comparable results. As a reference, a line indicating the anticipated tip radius model is given (for details see text).

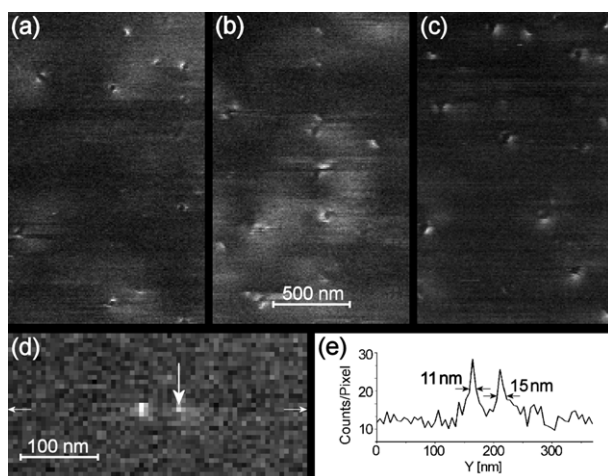


**Figure 4.** SNOM images with single molecule fluorescence patterns of Alexa 532 molecules distributed on a glass surface. The identical glass tip was covered with different metal layers: (a) 14 nm Al, (b) 27 nm Al and (c) 22 nm Ag. (To reduce noise, forth- and back-scans were combined.) (d) An enlarged single molecule pattern imaged as in (a) and a line scan across it. The image was scanned upwards, line by line from left to right. The molecule was photo bleached when the tip moved over the dye molecule at the position marked by the vertical arrow: the fluorescence stayed at the background signal for the following pixels. This is a typical feature of single molecule imaging.

account. A closer inspection of the images reveals that the distance between the double peaks, their widths as well as their signal-to-background ratio degrades when enhancing the Al layer from 14 nm (figure 5(a)) to 27 nm (figure 5(b)),

**Table 1.** Comparison of results for different metal layers.

Metal coating (nm)	Inclination angle (deg)	Peak distance <sup>a</sup> (nm)	Peak width <sup>a</sup> (nm)	Tip radius (nm)	Max. signal (kc s <sup>-1</sup> )	Background signal (kc s <sup>-1</sup> )
14 Al	12	47 (30)	15 (24)	25 <sup>b</sup>	47	5.4–15
27 Al	5	68 (45)	27 (34)	38 <sup>c</sup>	50	7.4–21
41 Al		(59)	(44)	52 <sup>c</sup>	7.4	2.5–3.9
22 Ag	5	58 (40)	31 (30)	33 <sup>c</sup>	126 <sup>d</sup>	27–41 <sup>d</sup>

<sup>a</sup> Values are mean values of several patterns. Parenthesis: calculated from model, excitation only.

<sup>b</sup> Estimated from a scanning electron micrograph.

<sup>c</sup> Calculated from layer thickness.

<sup>d</sup> At half of the illumination power of the other measurements.

a finding consistent with the calculations. However, it was surprising that good imaging results could be obtained with the 22 nm Ag layer at a middle inclination angle of only 5° (the calculated optimal angle of 23° could not be tested with our setup). A detailed description and analysis of the various measured parameters is given in table 1, where a minimal peakwidth of 15 nm could be verified for an Al coated probe (metal coating thickness = 14 nm, illumination angle 12°). This criterion is commonly used as an estimate of optical resolution [4, 6, 19, 20]. Experiments with 5 nm aluminium tips showed no near-field effects at all, a fact which indicates an experimental lower limit of the aluminium layer thickness which is probably caused by the formation of an oxide layer in air.

In contrast to these experiments with rather thin metallic coatings (<30 nm), we found that upon coating the identical

**Table 2.** Properties of different probes measured at single molecules or quantum dots.

Probe/publication		Single molecule pattern	Peak width (nm)	Signal-to-background ratio
This work		Double/single peaks	15/20	4
Completely Al (60 nm) covered quartz tip	[6]	Single peaks	32	5 <sup>a</sup>
Aperture less silicon tip	[4]	(Quantum dot:) single peak	10	0.2
Tip-on-aperture probe	[3]	Double peaks	10	5
Triangular aperture probe	[20]	Single/double/triple peaks	30	15 <sup>a</sup>
Aperture probe, illumination-collection mode	[19]	Single peak	22 <sup>a</sup>	6 <sup>a</sup>

<sup>a</sup> Estimate from cross-sections shown in the publications.

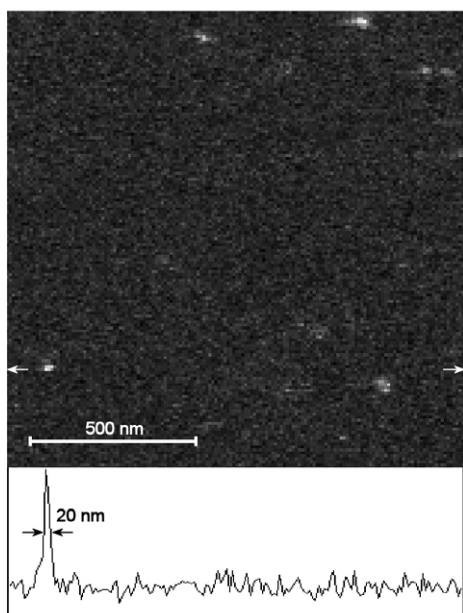


**Figure 5.** Single Alexa 532 dye molecules imaged with an optical probe coated with 30 nm Al. The plot shows a cross-section along the line marked by arrows. The fluorescence patterns are single peaks with a peak width of 20 nm, which is smaller than expected from the calculations for symmetrical illumination.

glass tip with 41 nm Al and 55 nm Ag, the experiment suffered from a limited light throughput which made single molecule fluorescence imaging impossible.

Our values compare very favourably with other published data in the field of high resolution SNOM imaging of single molecules or quantum dots (table 2). Moreover, our approach allows combination of high resolution imaging at a reasonable signal-to-background ratio with batch production due to its simplicity. A further interesting issue is the physical origin of the light confinement at the tip apex, as discussed in recent publications [12–14]. In the case of plasmonic waveguide excitation, a strong dependence of the imaging characteristics on the illumination angle is expected. This has been verified in our experiments since these optical probes revealed that already a slight adjustment of the illumination conditions can induce a more or less asymmetric single molecule fluorescence pattern. In certain cases, the setup could be tuned in a way that only one peak per dye molecule could be detected. This phenomenon allowed high resolution imaging of single dye molecules even with rather ‘thick’ metal layers, as shown in figure 5. Individual dye molecules could reproducibly be

imaged with a 30 nm Al coated glass tip, exhibiting single fluorescent spots with a FWHM of 20 nm.

## 5. Summary

We have shown that high resolution single molecule fluorescence SNOM imaging is possible at an optical resolution of 15 nm with optimized, apertureless and back-illuminated metal coated full body glass tips. The inclination angle of the illumination, the coating material and coating thickness have been optimized according to a theoretical multiple multipole calculation. Optimal coating thicknesses were determined to be about 10–15 nm for aluminium and 15–25 nm for silver. In addition, we found a subtle dependence of the observed single molecule fluorescence pattern on the illumination conditions, which might indicate the involvement of plasmon-coupled electric field tip enhancement as predicted in theoretical considerations.

This development will facilitate future experiments requiring optical high resolution imaging of functional single biomolecules under physiological conditions.

## Acknowledgments

The authors acknowledge and appreciate helpful discussions with B Hecht and Th Enderle.

## References

- [1] Hecht B, Sick B, Wild U P, Deckert V, Zenobi R, Martin O J F and Pohl D W 2000 *J. Chem. Phys.* **112** 7761–74
- [2] Hamann H F 2001 *Z. Phys. Chem.* **215** 1025–42
- [3] Frey H G, Witt S, Felderer K and Guckenberger R 2004 *Phys. Rev. Lett.* **93** 200801
- [4] Gerton J M, Wade L A, Lessard G A, Ma Z and Quate S R 2004 *Phys. Rev. Lett.* **93** 180801
- [5] Hartschuh A, Beversluis M R, Bouhelier A and Novotny L 2004 *Phil. Trans. R. Soc. A* **362** 807–19
- [6] Eckert R, Freyland J M, Gersen H, Heinzelmann H, Schürmann G, Noell W, Stauffer U and de Rooij N F 2000 *Appl. Phys. Lett.* **77** 3695–7
- [7] Aeschimann L, Akiyama T, Stauffer U, De Rooij N F, Thiery L, Eckert R and Heinzelmann H 2003 *J. Microsc.* **209** 182–7
- [8] Vaccaro L, Aeschimann L, Stauffer U, Herzog H P and Dändliker R 2003 *Appl. Phys. Lett.* **83** 584–6
- [9] Novotny L, Pohl D W and Hecht B 1995 *Ultramicroscopy* **61** 1–9
- [10] Keilmann F 1999 *J. Microsc.* **194** 567–70
- [11] Liu L and He S 2005 *Appl. Opt.* **44** 3429–37
- [12] Stockmann M I 2004 *Phys. Rev. Lett.* **93** 137404

- [13] Bouhelier A, Renger J, Beversluis M R and Novotny L 2003 *J. Microsc.* **210** 220–4
- [14] Janunts N A, Baghdasaryan K S, Nerkararyan Kh V and Hecht B 2005 *Opt. Commun.* **253** 118–24
- [15] Novotny L 1996 *Appl. Phys. Lett.* **69** 3806–8
- [16] Hagemann H-J, Gudat W and Kunz C 1974 *Deutsches Elektron-Synchrotron DESY SR-74/7*
- [17] Burke J J and Stegeman G I 1986 *Phys. Rev. B* **33** 5186–201
- [18] Haumann C, Toquant J, Pelargus Ch, Frey H G, Ros R, Pohl D W and Anselmetti D 2004 *Rev. Sci. Instrum.* **76** 033704–5
- [19] Hosaka N and Saiki T 2001 *J. Microsc.* **202** 362–4
- [20] Molenda D, Colas des Francs G, Fischer U C, Rau N and Naber A 2005 *Opt. Express* **13** 10688–96